Quantum Dots embedded in Graphene Nanoribbons by Chemical Substitution: Supporting Information

Eduard Carbonell-Sanromà,[†] Pedro Brandimarte,[‡,¶] Richard Balog,[†,§,‖] Martina Corso,[†,‡,§] Shigeki Kawai,[⊥,#,@] Aran Garcia-Lekue,[¶,§] Shohei Saito,[@,△] Shigehiro Yamaguchi,[▽] Ernst Meyer,[#] Daniel Sánchez-Portal,[‡,¶] and Jose Ignacio Pascual[*,†,§]

†*CIC nanoGUNE, Tolosa Hiribidea 76, 20018 Donostia-San Sebastian, Spain*

‡*Centro de Fisica de Materiales, 20018 Donostia-San Sebastian, Spain*

¶*Donostia International Physics Center, 20018 Donostia-San Sebastian, Spain*

§*Ikerbasque, Basque Foundation for Science, Bilbao, Spain*

‖*Department of Physics and Astronomy, Aarhus University, 8000 Aarhus C, Denmark*

⊥*99 International Center for Materials Nanoarchitectonics, National Institute for Materials Science, 1-1, Namiki, Tsukuba, Ibaraki 305-0044, Japan*

#*Department of Physics, University of Basel, CH-4056 Basel, Switzerland*

@*PRESTO, Japan Science and Technology Agency, Kawaguchi, Saitama 332-0012, Japan*

△*999 Department of Chemistry, Graduate School of Science, Kyoto University, Kitashirakawa Oiwake, Sakyo, Kyoto 606-8502, Japan*

▽*Institute of Transformative Bio-molecules, Nagoya University, Furo, Chikusa, Nagoya 464-8602, Japan*

E-mail: ji.pascual@nanogune.eu

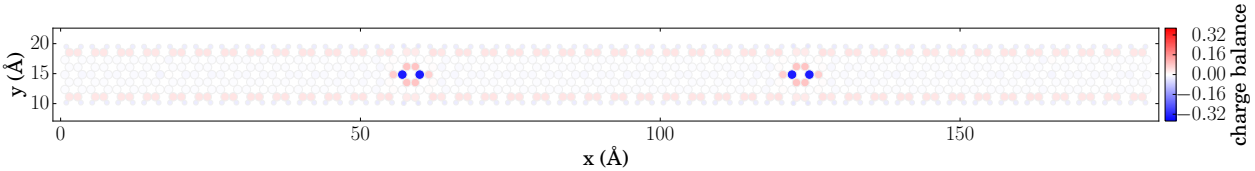

Figure S1: Mulliken population analysis of the freestanding hybrid 2B-7-AGNR. The boron atoms are negatively charged, receiving an amount of ∼0.38 electron charge from the neighbouring carbons which, in turn, are positively charged.

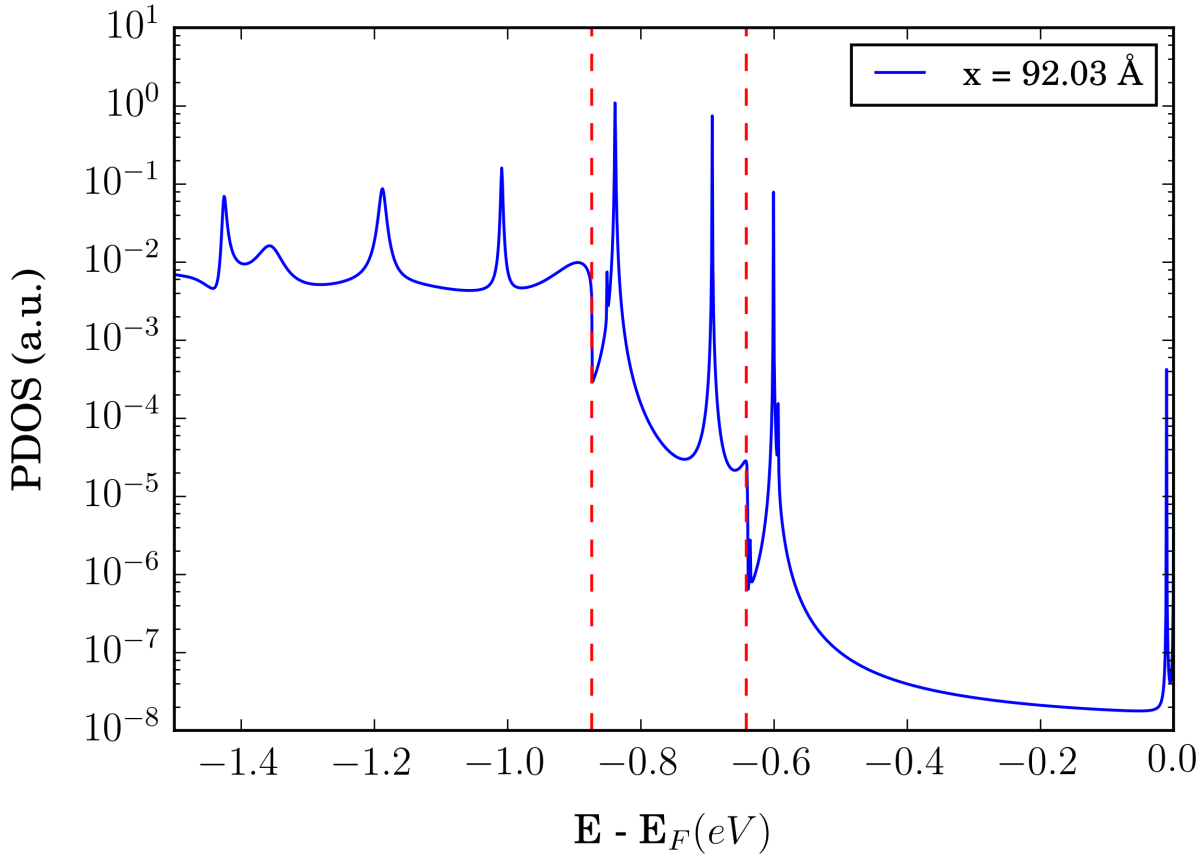

Figure S2: Projected DOS from a pristine segment enclosed between two borylated sections 6.5 nm apart. The plot is obtained at the middle position between the two borylated sections. The vertical dashed red lines correspond to onsets of the pristine VB (∼-0.64 eV) and VB-1 (∼-0.87 eV). With the log-scaled PDOS the increase of intensity coming from the VB-1 is clearly seen.

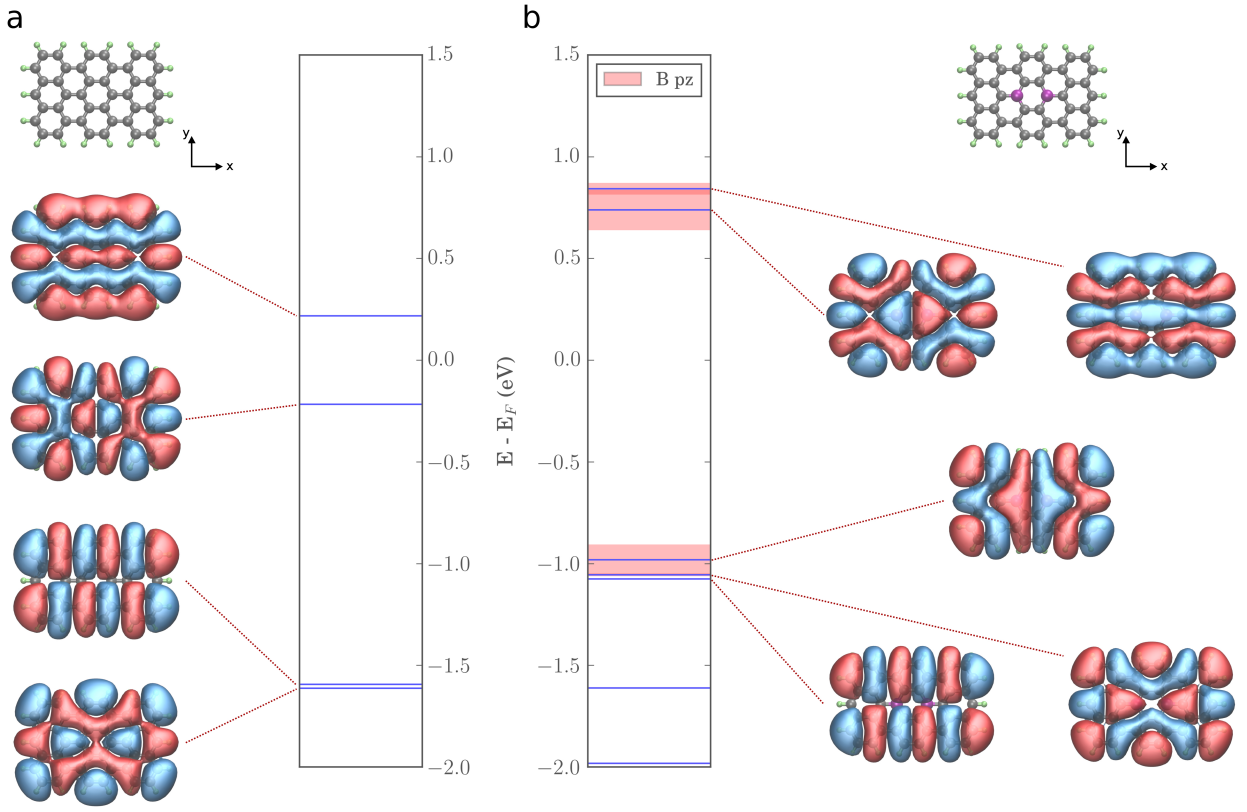

Figure S3: Wave functions and corresponding energy levels obtained for a pristine trisanthene molecule (a) and for a trisanthene molecule with a substituted pair of boron atoms (b). In the considered energy range, the boron-substituted molecule presents a new energy level (at $E-E_F = -0.98$ eV) with strong boron p_z character. The wave function of the boron induced level shows an even symmetry with respect to the mirror plane bisecting the molecule along x direction and an odd symmetry regarding the plane bisecting along y.

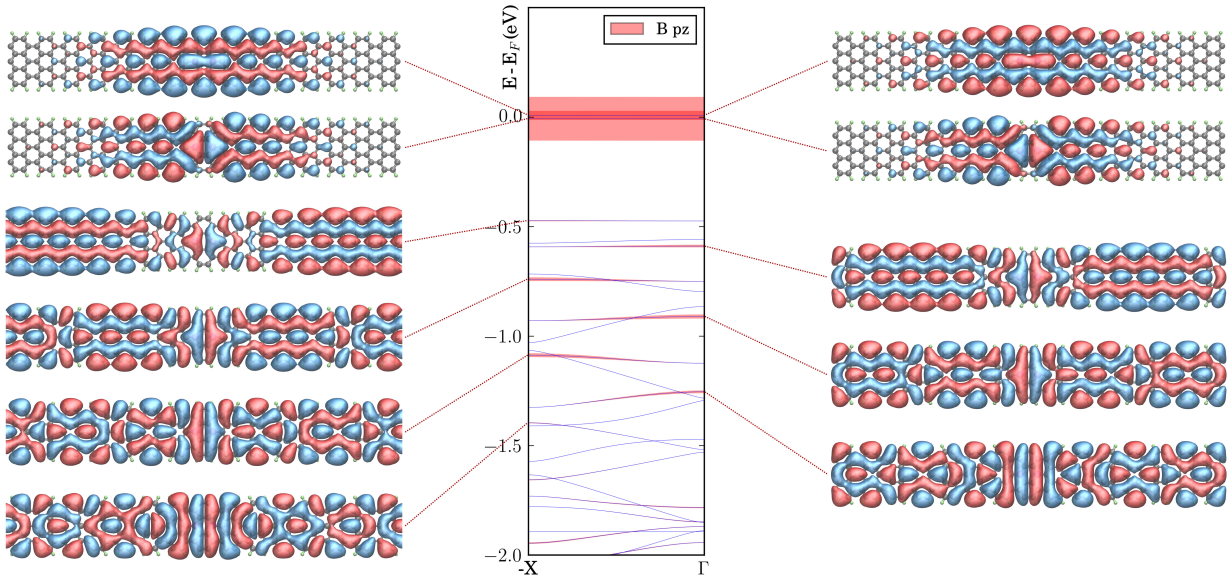

Figure S4: Band structure (center) obtained for a 7-AGNR with a periodic boron pair substitution. The unit cell of the ribbon has been chosen so that the distance between the boron dimer and its next periodic replica is equal to that of the open system calculation, namely 65 Å. Two defect levels, localized around the boron pair, are identified close to the Fermi energy. The band corresponding to the pristine nanoribbon valence band (VB) strongly hybridizes with a boron resonance and appears with a stronger boron p_z character alternately at Γ and -X points. This uneven k-point distribution is related to the nodal structure imposed by the relevant boron resonance shown in Fig S3. Due to this hybridization between the boron and carbon states, the VB is split into a collection of almost flat subbands and presents bigger gaps at the boundary of the Brillouin zone when compared to the VB-1. The corresponding wave functions are shown on the left for -X and on the right for Γ. One observes a nodal structure analogous to that of the eigenchannel wave functions calculated at the resonance energies. Starting with n=1 at -X ($E - E_F = -0.47$ eV), n=2 at Γ ($E - E_F = -0.59$ eV), and so forth, all these wave functions show an even symmetry with respect to the mirror plane bisecting the nanoribbon along its axis. Moreover, one notices that a phase change of π is imposed at the plane between the boron atoms, similarly to the boron induced state obtained in the isolated molecule calculation.

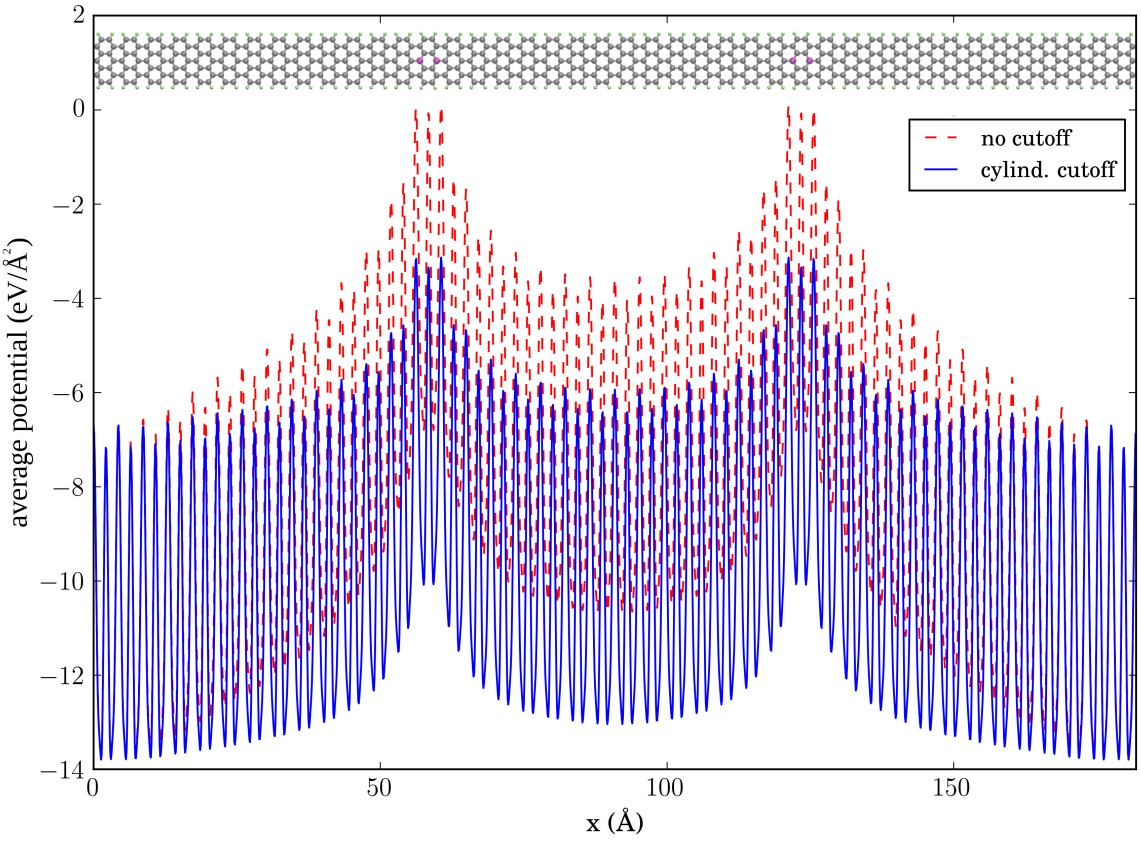

Figure S5: Laterally averaged electrostatic potential (Hartree potential plus local pseudopotential) obtained for the open system calculation of the hybrid 2B-7-AGNR, before (red) and after (blue) applying a cylindrical cutoff for the Coulomb interaction, with 12.5 Å cutoff radius. The small dipole created between the inner "quantum-well" and the outer "electrode" regions interacts via the long range part of the Coulomb potential with the periodic replicas along the directions perpendicular to the nanoribbon axis, even after considering a large vacuum region between them (we used a unit cell with 30 Å along both perpendicular directions). This artifact is removed after applying the cutoff, rendering the system really one-dimensional in spite of the periodic boundary conditions used in the calculations. The slow decay of the electrostatic potential around the boron defects is a signature of their small charging. Mulliken population analysis indicates that $0.37e$ charge is donated to each boron atom by the surrounding carbons (Figure S1). The remaining electrostatic background causes a small upward shift of the bands in the pristine confined segment of the hybrid 7-AGNR. As a result, the n=1 mode in Fig. 4a appears at -0.6 eV, a value higher than the onset of the pristine 7-AGNR bands and transmission step in Fig. 4b, at -0.64 eV. Since the n=1 mode lies above the bands injecting electrons in the 7-AGNR contacts, it cannot contribute to the transmission, and the first transmitting mode is the n=2, as seen in Fig. 4d. This effect is due to considering free-standing hybrid 7-AGNRs. In the experimental situation, the additional screening provided by the metal substrate is expected to eliminate this electrostatic background.

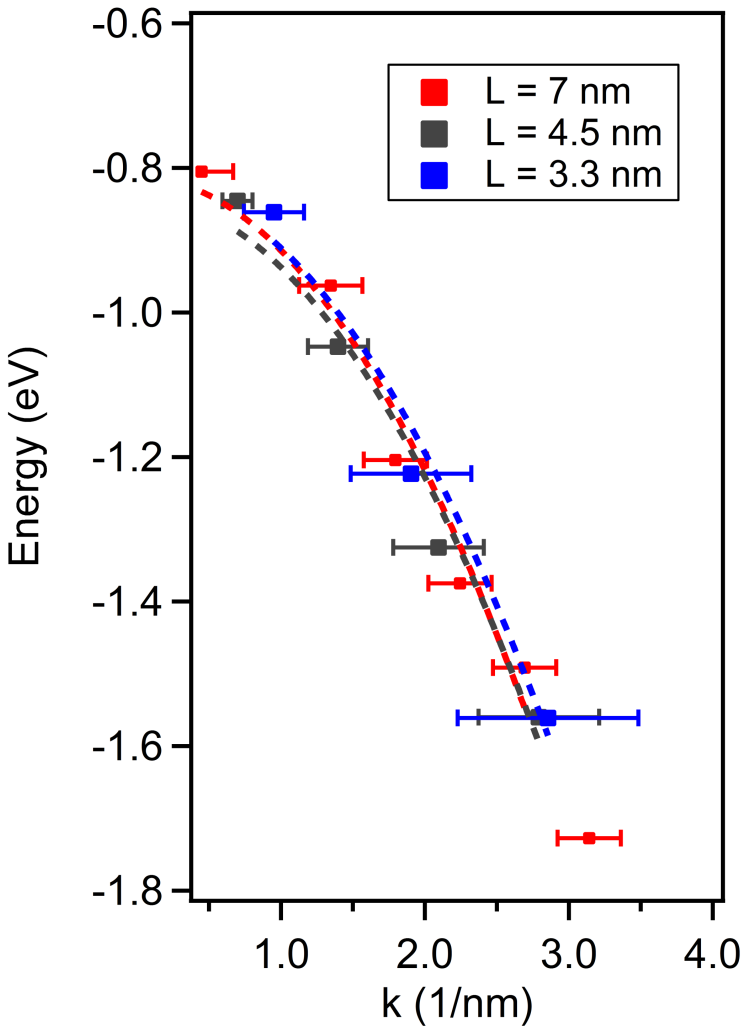

Figure S6: Energy dispersion relation ($k = n\pi/L$) for three quantum wells of different lengths. The data in red corresponds to the QW shown in Figure 3b of the manuscript for comparison. Dashed lines show parabolic fits to each data set, showing a good overlay of all energy dispersions.